nature communications

Article

https://doi.org/10.1038/s41467-024-52801-9

Transcriptional coactivator MED15 is required for beta cell maturation

Received: 30 July 2019

Accepted: 23 September 2024

Published online: 08 October 2024

Check for updates

Alex Z. Kadhim[1,2,3], Ben Vanderkruk[1,4], Samantha Mar[1,4], Meixia Dan[1,2,3], Katarina Zosel[1,4], Eric E. Xu[1,4], Rachel J. Spencer[1,2,3], Shugo Sasaki[1,4], Xuanjin Cheng[3], Shannon L. J. Sproul[1,4], Thilo Speckmann[1,4], Cuilan Nian[1,4], Robyn Cullen[3], Rocky Shi[1,4], Dan S. Luciani[1,4], Bradford G. Hoffman[1,4], Stefan Taubert[1,2,3] ✉ & Francis C. Lynn[1,4,5] ✉

Mediator, a co-regulator complex required for RNA Polymerase II activity, interacts with tissue-specific transcription factors to regulate development and maintain homeostasis. We observe reduced Mediator subunit *MED15* expression in endocrine hormone-producing pancreatic islets isolated from people living with type 2 diabetes and sought to understand how *MED15* and Mediator control gene expression programs important for the function of insulin-producing β-cells. Here we show that Med15 is expressed during mouse β-cell development and maturation. Knockout of Med15 in mouse β-cells causes defects in β-cell maturation without affecting β-cell mass or insulin expression. ChIP-seq and co-immunoprecipitation analyses found that Med15 binds β-cell transcription factors Nkx6-1 and NeuroD1 to regulate key β-cell maturation genes. In support of a conserved role during human development, human embryonic stem cell-derived β-like cells, genetically engineered to express high levels of MED15, express increased levels of maturation markers. We provide evidence of a conserved role for Mediator in β-cell maturation and demonstrate an additional layer of control that tunes β-cell transcription factor function.

Pancreatic islet β-cells that secrete insulin to maintain physiological blood glucose levels are destroyed or become dysfunctional in Type 1 (T1D) and Type 2 Diabetes (T2D), respectively. Although embryonic and neonatal β-cells produce insulin, their glucose responsiveness is blunted, and they secrete more insulin at lower glucose levels compared to adult β-cells; this elevated basal secretion may be required to facilitate rapid growth early in life[1]. Functional maturation, defined by glucose-stimulated insulin secretion (GSIS) in the adult physiological glucose range (5–10 mM), is accompanied by a number of changes to β-cell physiology. These include: (1) a shift from glycolysis to oxidative phosphorylation[2]; (2) a reduction in basal insulin secretion accompanied by a reduction in β-cell glucose sensitivity[2]; (3) reduced fasting insulin secretion and potentially a reduction in responsiveness to non-glucose secretagogues[2,3]; (4) reduced β-cell proliferation[4,5]; and (5) establishment of proper intra-islet paracrine interactions through the expression of Ucn3[1,6]. Maturation is also accompanied by an improved capacity to synthesize and store insulin, which may be facilitated by more efficient zinc-mediated crystallization in the secretory granule[7]. Functional maturation is achieved through the expression of transcription factors such as *Mafa*, *Pax6*, *NeuroD1*, *Nkx6-1*, *Errγ*, *Pdx1*, *Six2*, and *Six3*[8–14]. Mutations in some of these factors lead to monogenic forms of diabetes,

[1]Diabetes Research Program, BC Children's Hospital Research Institute, Vancouver, Canada. [2]Department of Medical Genetics, University of British Columbia, Vancouver, BC, Canada. [3]Centre for Molecular Medicine and Therapeutics, University of British Columbia, Vancouver, BC, Canada. [4]Departments of Surgery and Cellular and Physiological Sciences, University of British Columbia, Vancouver, Canada. [5]School of Biomedical Engineering, University of British Columbia, Vancouver, Canada. ✉e-mail: taubert@cmmt.ubc.ca; francis.lynn@ubc.ca

demonstrating the importance of proper transcriptional regulation for β-cell maturation[15].

Transcription factors exert their actions through RNA Polymerase II (Pol II). Thus, interactions that bridge DNA-bound transcription factors to RNA Pol II play a critical role in transcriptional regulation. Transcription factor function can be controlled by Mediator, a 25–31 subunit complex required for RNA Pol II-dependent transcription[16]. Mediator can change conformation based on its binding partners, and certain subunits can associate or dissociate without perturbing its core integrity[16–20]. Functionally, conformation changes allow Mediator to drive specific gene programs, and—depending on specific transcription factor-Mediator interactions—allow engagement at many different promoters[21,22]. Mediator is composed of four distinct modules: the head, middle, tail, and kinase modules[19,23,24]. Structure-function analyses in yeast have determined that the middle and head modules are essential for transcription, with the kinase and tail modules serving regulatory functions[18,25]. The tail module serves as a direct link to transcription factors[26,27], although transcription factors also contact Mediator subunits in other modules.

The tail module subunit Med15 is a conserved regulator of lipid metabolism through its interaction with sterol response element binding protein (SREBP-1)[28]. The Med15–SREBP-1 physical and functional interaction is conserved in *Caenorhabditis elegans*, with orthologs MDT-15 and SBP-1 regulating lipid metabolism and protecting against glucotoxicity[29]. Furthermore, *C. elegans* MDT-15 protects from hypoxia and oxidative stress through interactions with the transcription factors NHR-49 and SKN-1, orthologs of HNF4α and NRF2[30–33]. Notably, hypoxia and oxidative stress can also occur in β-cells of patients with T2D[34–36].

Because Med15 orthologs participate in these processes and interact with molecular partners relevant to β-cell development and maturation, we hypothesized that Med15—at least partly through its important role in Mediator—may act as a nexus that couples β-cell-specific transcription factors to core promoters to regulate β-cell maturation and function. In the present study, we demonstrate that Med15 is expressed in islets and that its expression is reduced in individuals with T2D. In mice, deletion of Med15 in β-cells resulted in severe glucose intolerance due to impaired β-cell maturation. We further show that Med15 is associated with unique regions of the genome that include consensus binding sites for several transcription factors essential for β-cell maturation, including Nkx6-1 and NeuroD1. Med15 can physically interact with these two transcription factors. Lastly, we genetically engineered human embryonic stem cells (hESCs) to express increased levels of MED15; β-like cells derived from these hESCs showed markers of improved β-cell maturation. Collectively, these data identify Mediator family member Med15 as a conserved β-cell coactivator required for efficient maturation.

Results

Med15 is expressed in mouse and human pancreatic cells and its expression is decreased in islets from individuals with T2D

As the role of Med15/Mediator has not previously been characterized in the pancreas, we performed qPCR and immunofluorescence analysis on mouse embryonic and adult pancreata. We found that *Med15* was highly expressed at E12.5–-E17.5 and in P1-8-week-old islets (Figs. 1A, S1). At E13.5, Med15 was nuclear and highly expressed in nascent insulin-positive β-cells but not in glucagon-positive α-cells (Fig. 1B). E18.5 staining demonstrated nuclear Med15 expression in some β-cells and in α-cells (Fig. 1C). Eight-week-old adult islets also showed nuclear Med15 expression (Fig. 1D) in both α- and β-cells. To confirm expression in human insulin-producing cells, we performed Western blots and readily detected Med15 expression in human and mouse islets, as well as in MIN6 insulinoma and hESC derived islet cells (Fig. 1E).

NanoString gene expression analysis of islets from donors diagnosed with T2D revealed that *MED15* expression was significantly decreased compared to islets from healthy donors, along with glucose sensing and metabolism genes such as glucose transporters GLUT1, GLUT2 (*SLC2A1*, *SLC2A2*), glucokinase (*GCK*), and hormones insulin (*INS*) and islet amyloid polypeptide (*IAPP*), suggesting a role for *MED15* and/or Mediator in adult β-cell function and pathogenesis of T2D (Supplementary Data 1; Figs. 1F, S2). Conversely, α-cell genes such as *GCG*, *ARX*, and *MAFB*; δ-cell genes *SST* and *MNX1*; and the early endocrine marker *NEUROG3* were unchanged or significantly increased in T2D (Figs. 1F, S2). These data show conserved expression of *MED15* in insulin-producing β-cells and suggest a role for *MED15* in β-cell development, maturation, or functional maintenance.

Med15 ablation impairs glucose tolerance and glucose-stimulated insulin secretion in mice

To test whether Med15 affects glucose homeostasis in vivo, we deleted it in nascent mouse β-cells using the $Ins1^{Cre}$ β-cell-specific knock-in line[37], generating M15betaKO mice (Fig. 2A). To control for gene dosage of insulin, control mice were $Ins1^{Cre/+}$; $Med15^{+/+}$ (CTRL) unless otherwise stated. We confirmed β-cell-specific knockout with immunofluorescence (Fig. 2B) and observed no change in body weight (Fig. S3A). Intraperitoneal glucose tolerance tests at 3, 6, and 8 weeks of age revealed that both male and female M15betaKO mice were glucose intolerant and had significantly reduced serum insulin levels (Figs. 2C, D, S3B–D), suggesting defective β-cell mass or function. To quantify β-cell mass, we performed morphometric analyses on pancreata of 8-week M15betaKO mice; we found that they showed no change in gross islet morphology, insulin-positive β-cells, glucagon-positive α-cells, or total pancreatic cells (Figs. 2E, S3F–H). However, we did observe a significant increase in β-cell proliferation in 3-week-old M15betaKO islets (Fig. S3E), which may indicate impaired β-cell maturation. To assess insulin secretion, we carried out perifusion experiments on islets of 8-week-old knockout mice. M15betaKO islets had impaired first- and second-phase insulin secretion yet displayed no difference in total insulin content (Figs. 2F, G, S3I, J). To bypass the early steps in GSIS, islets were stimulated with α-ketoglutarate or KCl. M15betaKO islets displayed normal insulin secretion with either secretagogue (Figs. 2F, S3I), suggesting a defect upstream of mitochondrial metabolism. Taken together, these data demonstrate that Med15 and/or Mediator is required for β-cell function.

Loss of Med15 impairs the expression of β-cell maturation genes and glucose uptake

To define how the loss of Med15 affects the islet transcriptome, we performed RNA-seq on islets from 8-week control ($Ins1^{+/+}$; $Med15^{fl/fl}$) and M15betaKO mice. The most significantly downregulated genes in M15betaKO islets included cytochrome c oxidase subunit VIa polypeptide 2 (*Cox6a2*) encoding a mitochondrial ETC component, β-cell maturation markers urocortin 3 (*Ucn3*) and transcription factor *Mafa*, glucose transporter *Slc2a2*/Glut2, and endoplasmic reticulum oxidoreductase 1β (*Ero1lb*), which is important for disulfide bond formation during insulin maturation (Supplementary Data 2; Fig. 3A)[38]. In agreement with the RNA-seq data, M15betaKO islets showed complete loss of Mafa, Ucn3, and Glut2 immunostaining (Fig. 3B), which are markers of glucose-responsive β-cells[1,12,39], at all stages tested (P1-8 weeks; Fig. S4). Collectively, these results demonstrate that M15betaKO islets fail to express key β-cell genes required for functional maturity. To assess a functional marker of immaturity, we studied insulin granule morphology in M15betaKO cells by electron microscopy. We found that M15betaKO islets have significantly fewer and smaller dense core insulin granules (Fig. 3C–E), indicating a lack of insulin granule and β-cell maturation, likely due to reduced Slc30a8 expression and impaired zinc concentration and insulin crystallization within the granules. These data show that Med15, potentially through its role within Mediator, is required for β-cell maturation.

https://doi.org/10.1038/s41467-024-52801-9

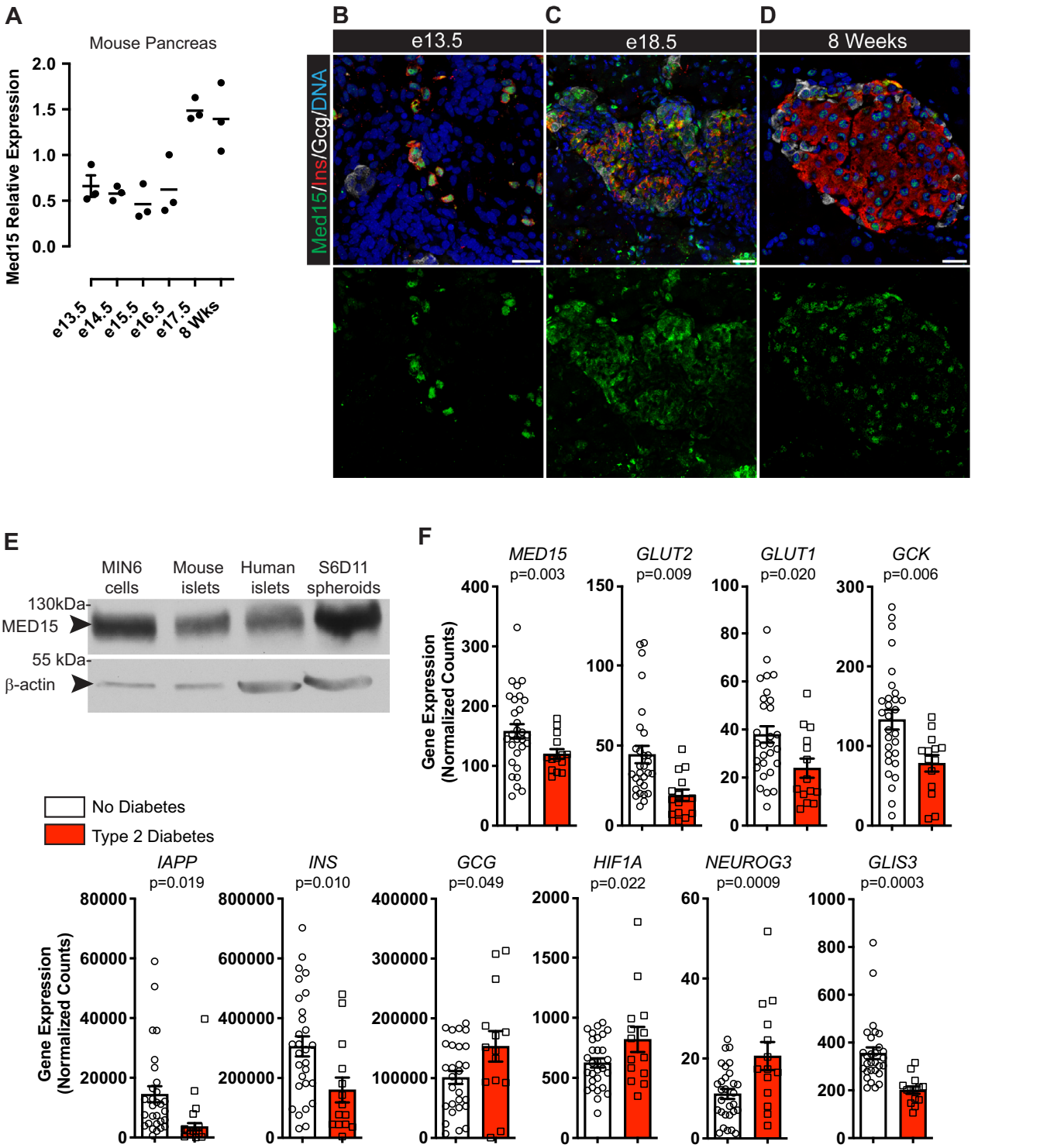

Fig. 1 | Med15 is expressed in β-cells and downregulated during type 2 diabetes. **A** qPCR of *Med15* expression in whole mouse pancreas from embryonic day (e) 13.5–17.5 and 8-week-old islets ($n = 3$ embryos from 3 litters); error bars represent mean ± SEM. **B**–**D** Immunofluorescence of Med15 (green), glucagon (GCG; cyan), insulin (INS; red), and nuclei (Hoechst; blue) in E13.5 (**B**), E18.5 (**C**), and 8-week-old (**D**) mouse pancreas (representative of $n = 3$ mice), scale bars = 25 μm. **E** Western blot of Med15 in MIN6, mouse and human islets, and stage 6 day 11 (S6D11) differentiated β-like cell spheroids (representative of $n = 3$ individuals or differentiations). **F** Normalized expression levels of selected significantly differentially expressed genes in islets isolated from healthy individuals (white bars; $n = 29$) or those living with T2D (red bars; $n = 14$). Exact *p*-values indicated under gene name by two-tailed Student's *t*-test; error bars represent mean ± SEM. Source data are provided as Source_Data.xlsx.

Because we observed reduced expression of mitochondrial proteins *Cox6a2* and *Ndufs2* and increased expression of *Ucp2* upon loss of Med15 (Supplementary Data 2), we next tested whether loss of Med15 impaired mitochondrial function. We found that islets from M15betaKO show reduced glucose-stimulated oxygen consumption (Fig. 3F), but no change in maximal respiration (Fig. 3G), suggesting no functional mitochondrial impairment. In agreement with the insulin secretion data, mitochondrial membrane potential, as measured by

https://doi.org/10.1038/s41467-024-52801-9

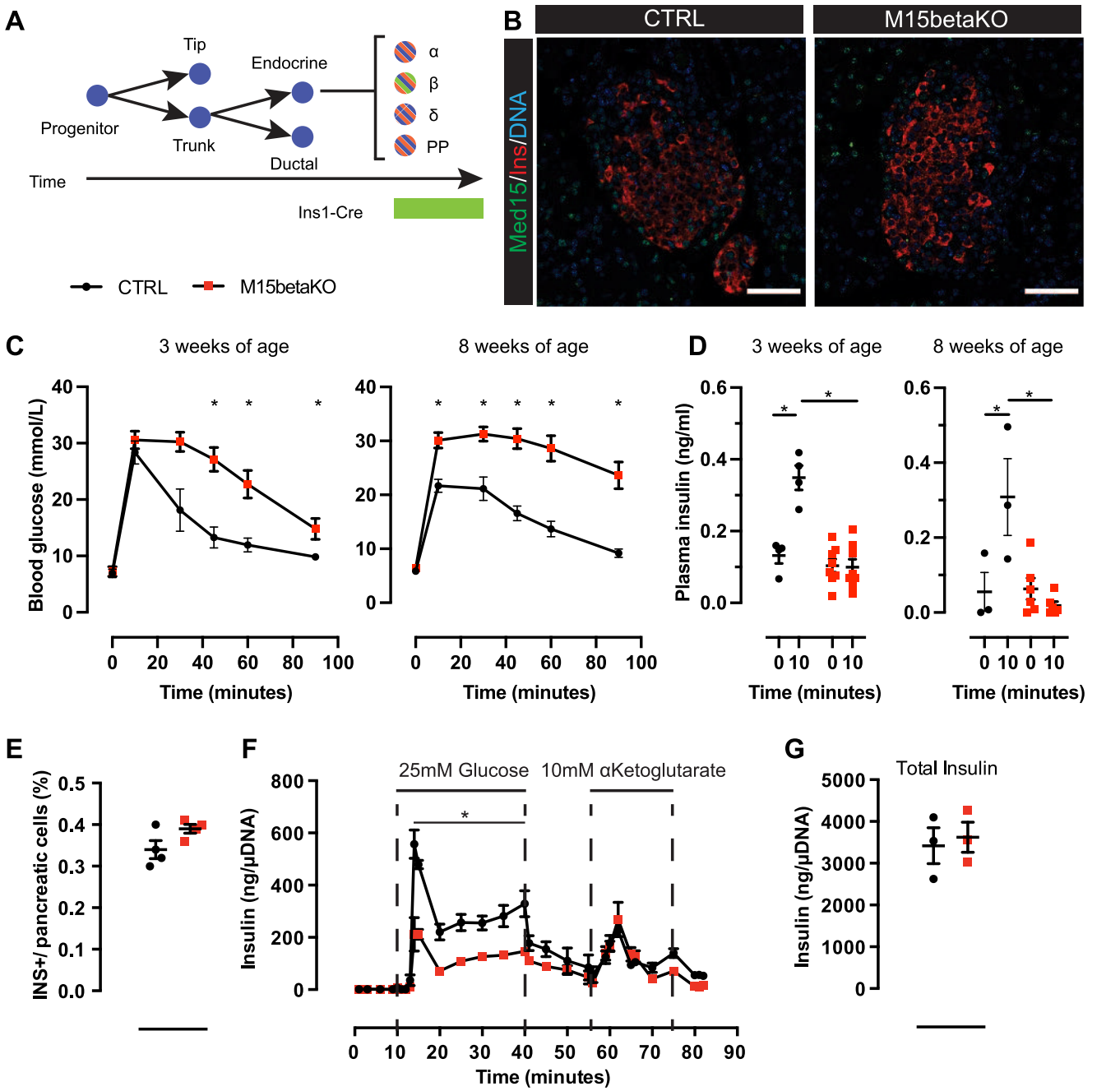

Fig. 2 | Med15 deletion in β-cells leads to glucose intolerance and impaired GSIS. A Schematic of *Ins1*-Cre mouse model used in experiments. **B** Immunofluorescent staining of Med15 (green), insulin (Ins; red) in 8-week-old control (CTRL= $Ins1^{Cre/+}$; $Med15^{+/+}$) and knockout (M15betaKO= *Ins1Cre/+*; $Med15^{fl/fl}$) mouse pancreas sections (representative of $n = 3$ mice; scale bars = 50 μm). **C** Intraperitoneal glucose tolerance of 3- and 8-week CTRL (black circles; $n = 4$ and $n = 4$ mice, respectively), and M15betaKO mice (red squares; $n = 8$ and $n = 8$ mice, respectively); $^*p \le 0.05$ by ANOVA with Sidak post-test. **D** Serum insulin measurements at time 0 and 10 min of (C) in 3- and 8-week CTRL (black circles; $n = 4$ and $n = 3$ mice, respectively), and M15betaKO mice (red squares; $n = 8$ and $n = 6$ mice, respectively), $^*p \le 0.05$ by ANOVA with Sidak post-test. **E** Quantification of β-cells as determined by insulin immunofluorescence per DAPI+ pancreatic cells in CTRL (black circles) and M15betaKO (red squares) mice ($n = 4$ mice). **F** Normalized insulin secretion from perifusion assay of 8-week CTRL (black circles) and M15betaKO (red squares) mouse islets stimulated with 25 mM glucose and 10 mM α-ketoglutarate ($n = 3$ mice); $^*p \le 0.05$ by ANOVA with Sidak post-test. **G** Total insulin measured from islets in (**F**) from CTRL (black circles) and M15betaKO (red circles) mice as measured by ELISA ($n = 3$ mice). Throughout, error bars represent mean ± SEM. Source data are provided as Source_Data.xlsx.

fluorescent probe tetramethylrhodamine ethyl ester (TMRE) normalized to mitochondrial mass marker MitoTracker Green (MTG) (Fig. S5A), was significantly reduced in islets from M15betaKO mice upon stimulation with glucose, but not following stimulation with the mitochondrial substrate α-ketoglutarate (Fig. S5B). To examine possible differences in mitochondrial networking, we analyzed three-dimensional mitochondrial morphology in control and M15betaKO islets using confocal microscopy. This revealed reduced mitochondrial count per cell (Fig. S5C, D) yet increased mitochondrial volume (Fig. S5E) in islets from M15betaKO mice, suggesting altered mitochondrial fission/fusion dynamics that likely result from β-cell immaturity.

As islets from M15betaKO mice have significantly reduced Slc2a2 expression levels (Figs. 3B, S4), we tested whether they showed normal

https://doi.org/10.1038/s41467-024-52801-9

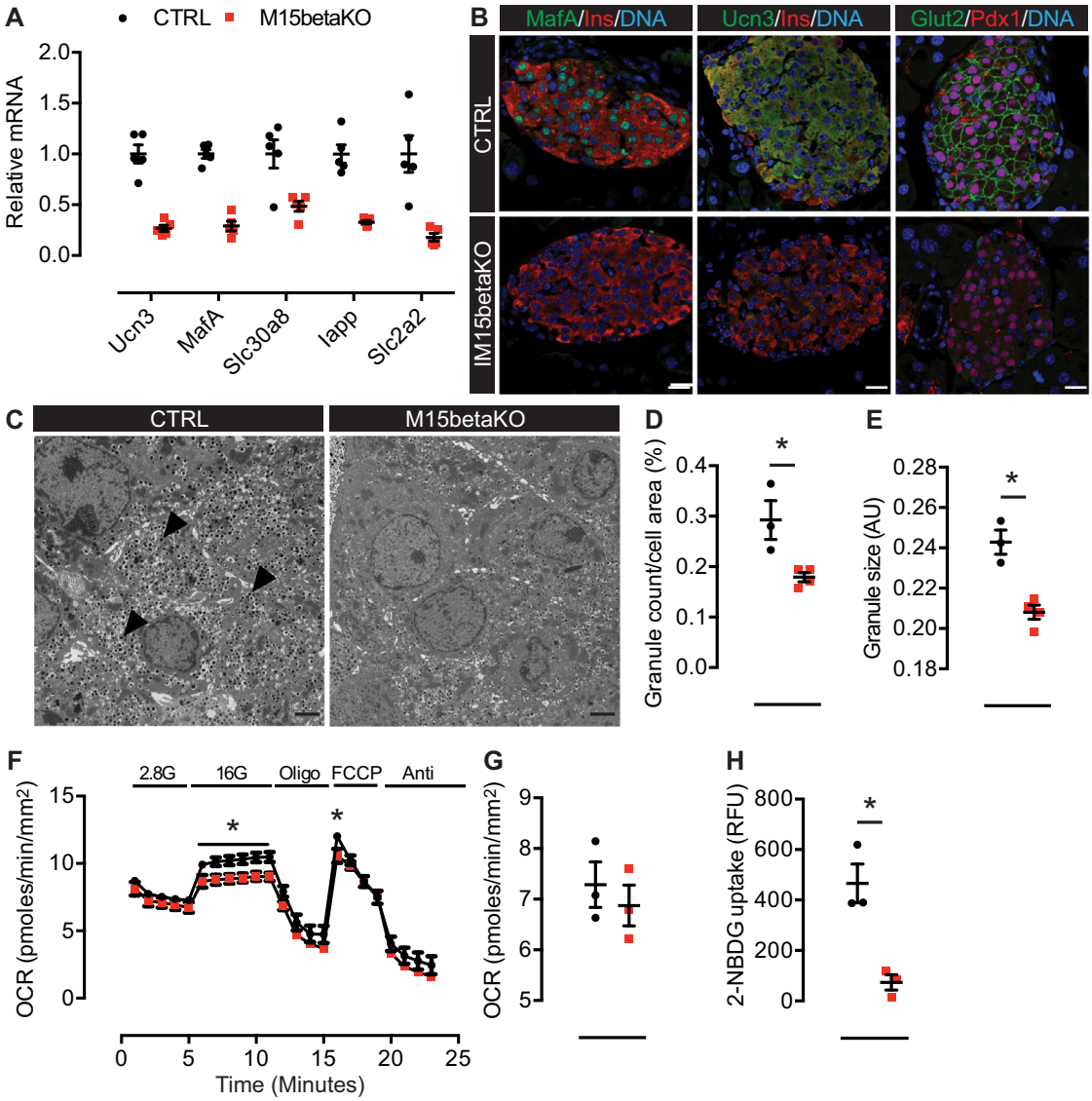

Fig. 3 | Med15 is required for expression of β-cell maturation genes. A Bulk RNA-seq expression for select β-cell maturation genes of 8-week control (black circles; *Ins1*$^{+/+}$;*Med15*$^{fl/fl}$) versus M15betaKO (red squares) islets ($n = 5$ mice). **B** Immunofluorescence of 8-week control versus knockout mouse pancreatic sections (representative of $n = 3$ mice), scale bars = 25 μm. **C** Transmission electron microscopy of 8-week control and knockout islets, arrowheads represent mature insulin secretory granules (representative of $n = 3$ CTRL, $n = 4$ M15betaKO mice) scale bars = 2 μm. **D** Quantification of mature insulin secretory granules from (**C**) ($n = 3$ CTRL, black circles; $n = 4$ M15betaKO, red squares), $^*p \le 0.05$ by unpaired two-tailed Student's *t*-test. **E** Quantification of mature insulin secretory granule size from (**C**) ($n = 3$ CTRL, black circles; $n = 4$ M15betaKO, red squares), $^*p \le 0.05$ by unpaired two-tailed Student's *t*-test. **F** Seahorse assay measuring mitochondrial function as oxygen consumption rate (OCR) per area of islets in control (black circles) and M15betaKO (red squares) samples (islets from $n = 3$ mice); $^*p \le 0.05$ by two-way ANOVA with Sidak multiple-comparison test. **G** Maximal respiration (after addition of FCCP) normalized to basal OCR in control (black circles) and M15betaKO (red squares) islets (islets from $n = 3$ mice). **H** Glucose uptake as measured by glucose analog 2-NBDG in 8-week control (black circles) and M15betaKO (red squares) dispersed islets (islets from $n = 3$ mice), $^*p \le 0.05$ by unpaired two-tailed Student's *t*-test. Throughout, error bars represent mean ± SEM. Source data are provided as Source_Data.xlsx.

glucose uptake. Studying dispersed islets incubated with the fluorescent glucose analog 2-NBDG, we found that M15betaKO had impaired glucose uptake compared to control islets (Fig. 3H). These data support and provide a mechanistic understanding of the significant reduction in GSIS in M15betaKO islets (Fig. 2F). Altogether, we find that loss of Med15, and potentially Mediator function, in nascent β-cells, leads to impaired glucose uptake and impaired functional maturation.

Med15 cooperates with β-cell transcription factors to regulate the β-cell transcriptome

As highlighted above, expression of mature β-cell markers *Ucn3* and *Mafa* and genes encoding key metabolic machinery such as *Slc2a2*, *Ero1lb*, and *G6pc2* were reduced in *Med15*-deficient islets (Figs. 3, 4A, S4, S5). Gene set enrichment analysis identified β-cell hallmark genes as the most strongly impaired gene set following *Med15* knockout in β-cells (Fig. 4B). Moreover, downregulation of the unfolded protein response and protein secretion and glycolysis pathways (Fig. 4B) support a transcriptional basis underlying decrements in mature insulin granule density (Fig. 3C–E) and insulin secretion we observed in M15betaKO β-cells (Fig. 2F); whereas, reduced steady-state expression of cell cycle-regulating genes in the G2/M checkpoint and E2F target gene sets (Fig. 4B) suggest a transcriptional basis for the increase in cell replication (Fig. S3E). Reduced expression of the mTOR and AKT pathways, which facilitate β-cell maturation in response to dietary stimuli, further indicates an immature transcriptional phenotype in

https://doi.org/10.1038/s41467-024-52801-9

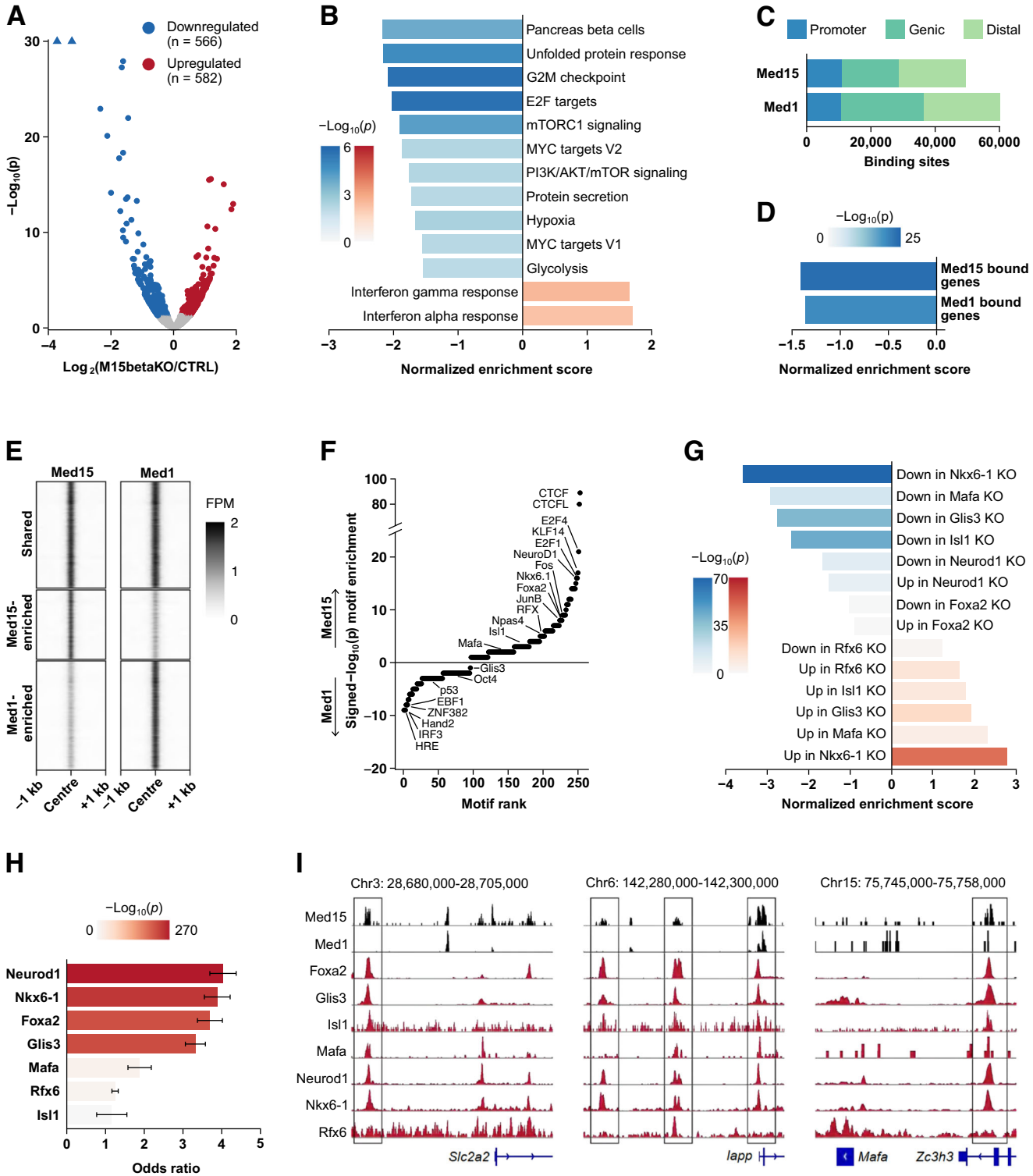

M15betaKO islets[40,41]. On the other hand, genes of the interferon response, associated with compromised β-cell function in T1D and T2D, were upregulated in M15betaKO islets (Fig. 4B)[42,43]. These data indicate an essential role for MED15 in establishing the mature β-cell transcriptome.

To more directly link Med15 activity with the regulation of β-cell gene expression, we mapped binding locations of Med15 and the Mediator middle module subunit Med1 in MIN6 mouse insulinoma cells using ChIP-seq[44,45]. We identified 47,544 genomic sites bound by Med15 and 58,193 sites bound by Med1, with roughly 10,000 of each mapping to gene promoters (Fig. 4C). Binding sites were significantly enriched at annotated gene promoters and distal enhancers (Fig. S6A). Importantly, genes with promoters targeted by Med15 tended to be downregulated in M15betaKO islets (Fig. 4D). Similarly, genes downregulated in M15betaKO islets were enriched with promoter-bound Med15, whereas upregulated genes were depleted (Fig. S6B), together supporting a role for Med15 in increasing target gene expression in β-cells. A similar pattern was observed for Med1-bound genes (Figs. 4D, S6B), consistent with the expectation that Med1 operates within the Mediator complex. Notably, we observed imperfect overlap of Med15

Fig. 4 | Med15 cooperates with mature beta cell transcription factors to regulate gene expression. A Volcano plot comparing gene expression in M15betaKO and CTRL islets ($n = 5$ mice); p-values calculated using Wald tests; blue = downregulated; red = upregulated. **B** Enrichment analysis of Hallmark gene sets in M15betaKO vs. CTRL islet transcriptomes. Gene sets depleted in M15betaKO islets are shown in blue and gene sets enriched in M15betaKO are shown in red; p-values calculated using permutation tests with Benjamini–Hochberg correction. **C** Distribution of Med15 and Med1 binding site annotations in MIN6 cells ($n = 3$ independent ChIP experiments); blue = promoters; dark green = genic regions; light green = distal regions. **D** Enrichment analysis of genes with Med15 or Med1 bound at their promoters in M15betaKO vs. CTRL islet transcriptomes ($n = 3$ independent ChIP experiments). **E** Heatmaps of ChIP-seq signal at Med15 and Med1 binding sites in MIN6 cells. The heatmap is segregated into sites where peaks were statistically defined for both (shared) or for only one factor. FPM, fragments per million ($n = 3$ independent ChIP experiments). **F** Transcription factor binding motifs enriched in Med15 and Med1 binding sites. A positive signed -log10(p-value) indicates the motif is enriched in Med15 binding sites compared to Med1 binding sites. p-values calculated using HOMER v4.11.1; only motifs with $p < 0.05$ (Benjamini–Hochberg correction) are plotted. **G** Enrichment analysis of genes differentially expressed in published KO models in IM15KO vs. CTRL islet transcriptomes; p-values calculated using permutation tests with Benjamini–Hochberg correction. **H** Bar plot shows the mean odds ratios that Med15-bound promoters significantly overlap with promoters bound by the indicated transcription factors. Odds ratios greater than 1 indicate Med15 binds to promoters that are also bound by the transcription factor more frequently than expected by chance. Error bars indicate the 95% confidence intervals of the mean; p-values calculated using two-sided Fisher's exact tests with Benjamini–Hochberg correction. **I** ChIP-seq tracks of Med15, Med1, Foxa2, Glis3, Isl1, Mafa, Nkx6-1, Neurod1, and Rfx6 at the *Slc2a2*, *Iapp*, and *Mafa* gene loci. Source data are provided as Source_Data.xlsx.

and Med1 binding sites in MIN6 cells (Fig. 4E), suggesting that target specificity by Mediator may be influenced by the inclusion or exclusion of Med15.

Because Med15 is a subunit of the tail module, which interacts directly with some sequence-specific transcription factors, we investigated whether known DNA binding motifs were enriched in Med15-bound loci. Motifs targeted by CTCF, E2F family proteins, the activity-regulated factors Fos, JunB and Npas4, and, notably, the mature β-cell transcription factors Nkx6-1, NeuroD1, Foxa2, Isl1, and Mafa, were overrepresented in Med15 footprints (Fig. 4F). To test if these transcription factors cooperate with Med15 to regulate target gene expression, we compared the gene expression changes in M15betaKO islets with gene expression changes following deletion of transcription factor genes identified in the motif analysis for which transcriptome data is published[9,11,46–50]. Genes that were dysregulated due to the deletion of *Nkx6-1*, *Mafa*, *Glis3*, *Isl1*, *Neurod1*, and *Rfx6* were enriched in the genes dysregulated due to the deletion of *Med15* (Fig. 4G). This finding is consistent with the idea that these transcription factors cooperate with Med15 to regulate gene expression, and highlighted the Nkx6-1 regulon as most similar. Next, we compared our ChIP-seq data with available ChIP-seq data of the same transcription factors in mouse islets or β-cell lines[9,11,46–50]. The set of genes directly targeted by Med15 and by Neurod1, Nkx6-1, Foxa2, and Glis3 strongly overlapped (Fig. 4H, I). Further, the binding intensity of each of these transcription factors was higher at promoters and enhancers where Med15 was also bound compared to promoters and enhancers bound by the transcription factor but not by Med15 (Fig. S4C). Together, these data suggest that multiple transcription factors in β-cells interact with Med15 to regulate Mediator activity and target gene expression.

The combination of DNA binding motif enrichment, transcriptome similarity, and genome-wide binding prioritized Nkx6-1 as a likely interactor of Med15. To test whether Med15 and specific transcription factors interact physically, we performed co-immunoprecipitation in MIN6 cells. We found that Med15 interacts with Nkx6-1 and NeuroD1 in MIN6 cells (Fig. 5A, B). This interaction appears to be specific to Med15 because the middle module subunit Med1 did not co-immunoprecipitate Nkx6-1 (Fig. 5A). Further analysis revealed that immobilized Nkx6-1 co-purifies with Med15, Med6, and Med12, but not with Med23 (Figs. 5C, Fig. S7A) and the Med15:Nkx6-1 interaction can be recapitulated in vitro with purified proteins (Fig. 5D). This may reflect a specific Mediator conformation or loss of Med1 and/or Med23 during purification; we note that Med15 co-purified with Med6, Med12, and Med23 in MIN6 lysates (Fig. S7B), suggesting the presence of canonical Mediator complex in these cells.

To test whether this interaction occurred in the absence of other factors, we tested the ability of purified, Flag-tagged MED15 to interact with purified, HA-tagged Nkx6-1 in vitro. We observed a specific interaction between Med15 and Nkx6-1 with multiple different protein preparations (Fig. 5D). Finally, we used AlphaFold and AlphaPulldown to model protein-protein interactions between the domains of MED15 and NKX6.1. We found two regions of potential interaction between MED15 and NKX6.1 (Figs. 5E, S8) and found that MED15 may interact with other important β-cell transcription factors, including PAX6 and NEUROD1 (Fig. S8)[51,52]. In sum, these data suggest that Med15 helps to coordinate Mediator interactions with multiple transcription factors at specific loci to induce critical β-cell maturation genes during β-cell maturation.

Elevated expression of MED15 in human embryonic stem cell-derived β-cells improves expression of maturation markers

To test if MED15 plays a role in human β-cell maturation, we used CRISPR/Cas9 genome editing to knock a *2A-mScarlet-MED15* expression cassette onto the *INS* coding region in H1 hESCs to generate a MED15 beta cell over-expression model (MED15betaOE) (Fig. S9A)[53–55]. These hESCs were then differentiated to stage 6 immature pancreatic β-cells[54–56]. MED15 overexpression did not alter β-cell differentiation as we obtained similar frequencies of insulin-expressing cells as in control differentiations (Figs. 6A, S9B). FAC sorted β-cells from these spheroids robustly expressed RFP/mScarlet and *MED15* (Figs. 6B, S9B). Additional gene expression analysis revealed that MED15betaOE spheroids expressed higher levels of several markers of β-cell maturation, including *UCN3* (Fig. 6C), IAPP (Fig. 6D), *INS*, and *SLC30A8* (Fig. 6F), but not *NKX6.1* (Fig. 6E). Interestingly, five of the genes increased in MED15betaOE cells are bound and regulated by Med15 in murine islets, including *SLC30A8*, *UCN3*, *IAPP*, and *G6PC2*. Immunostaining indicated significantly higher levels of UCN3 expression in MED15betaOE insulin-expressing cells (Fig. 6G). These data demonstrate that MED15 plays a conserved role in human β-cells where it also increases the expression of markers of β-cell maturation.

Discussion

Transcription factors and regulatory networks play essential roles in the development, differentiation, maturation, and function of the pancreatic β-cells[57–60]. However, how individual transcription factors interface with RNA Pol II and whether these interactions can be harnessed to promote β-cell maturation has not been studied. Here, we demonstrate that the transcriptional coactivator Med15, a subunit of the evolutionarily conserved Mediator complex, is essential for β-cell maturation. We show that Med15 interacts with Nkx6-1, a transcription factor known to drive β-cell maturation[11] and that Med15 occupies and regulates genes alongside β-cell transcription factors, including Nkx6-1. Notably, this includes numerous genes required for insulin secretion and biosynthesis, including *Mafa*, *Slc2a2*, *Slc30a8*, and *G6pc2*. Consequently, reductions of Med15 compromise glucose uptake, impair insulin granule maturation and result in impairments in organismal glucose homeostasis and subsequent glucose intolerance. Collectively, our data suggest a model whereby Med15, potentially through Mediator, coordinates transcriptional control of β-cell maturation.

https://doi.org/10.1038/s41467-024-52801-9

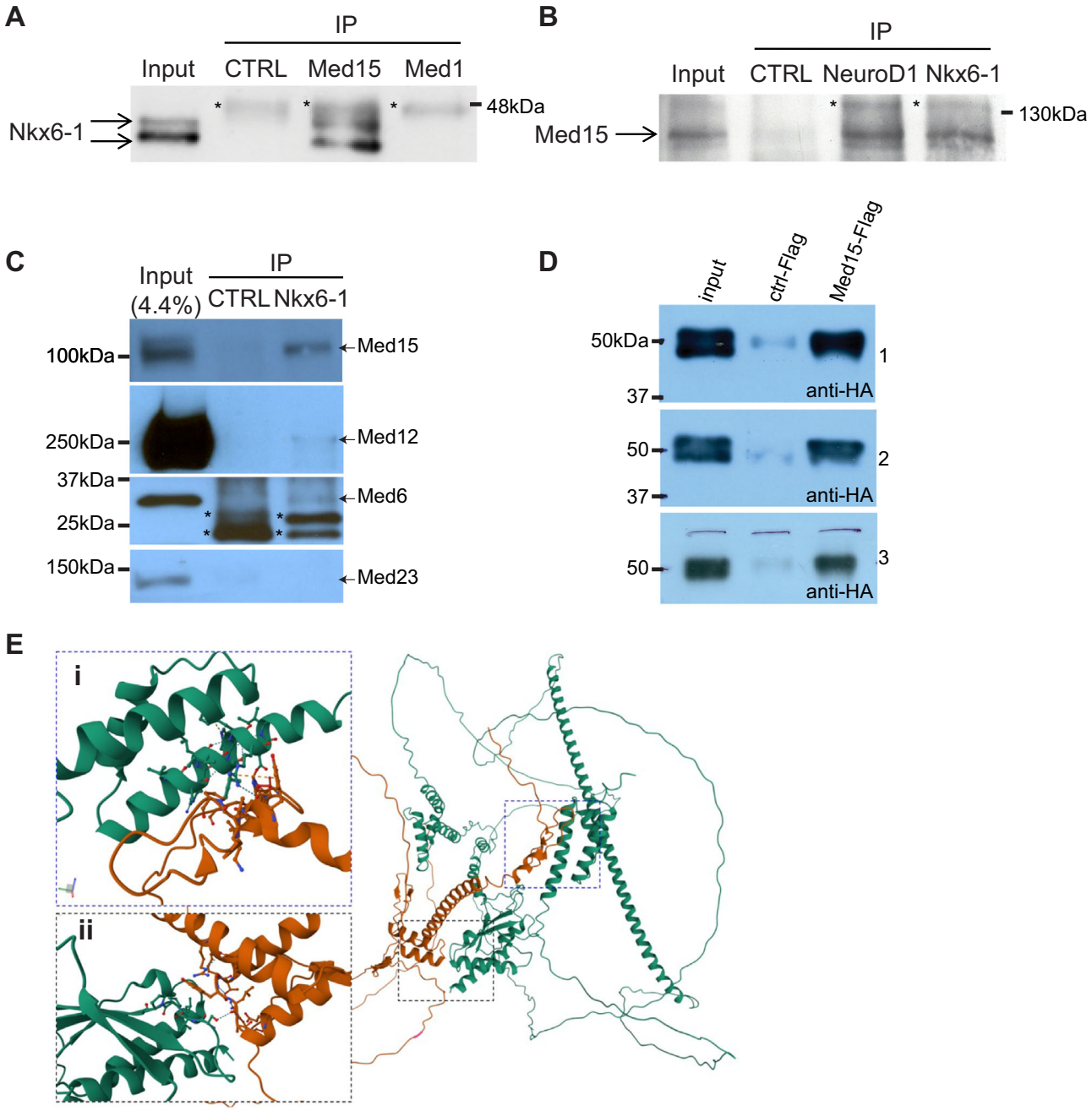

Fig. 5 | Med15 interacts with Nkx6-1 and Neurod1 to regulate β-cell maturation. **A** Co-immunoprecipitation of Med15 and Med1 with Nkx6-1 using mouse β-cell line (MIN6) lysates (representative of $n = 3$ biological replicates); CTRL = nonspecific IgG control using MIN6 cell lysates. **B** Co-immunoprecipitation of Med15 with NeuroD1 and Nkx6-1 using mouse β-cell line (MIN6) lysates (representative of $n = 3$ biological replicates); CTRL = nonspecific IgG control. **C** Co-immunoprecipitation of Med15, Med12, and Med6 with Nkx6-1 using mouse β-cell line (MIN6) lysates (representative of $n = 3$ biological replicates); CTRL = nonspecific IgG control. **D** In vitro interaction between HA-tagged Nkx6-1 and Flag-tagged Med15. Flag-tagged proteins (Med15 or control) were immobilized on a Flag affinity resin and then incubated with HA-tagged full-length Nkx6-1 prior to Western blotting using anti-HA antibodies ($n = 3$ biological replicates). **E** AlphaPulldown predicted interactions between domains of MED15 (green) and NKX6.1 (orange). Inset (i) MED15 helix subunit (amino acids 52–71) and NKX6.1 (amino acids 306–367) and (ii) MED15 (amino acids 740–787) and NKX6.1 (amino acids 240–290). In all panels, arrows = predicted molecular weight, * = nonspecific signal. Source data are provided as Source_Data.xlsx.

In our mouse model, we observed that conditional loss of Med15 in β-cells impaired glucose tolerance without affecting β-cell numbers. The observed hyperglycemia is likely caused primarily by defective β-cell glucose uptake. This is supported by our functional analyses, suggesting reduced mitochondrial function under high glucose conditions, driven solely by reduced glycolytic product availability. Subtle differences in mitochondrial morphology were also observed that mirror those seen in other knockout models with impaired β-cell maturation, including the reduced mitochondrial count of Nkx6-1 knockout islets and the increased mitochondrial volume in ERRγ knockout islets[61,62]. Downstream of β-cell glucose uptake, we demonstrate that several genes important for insulin biogenesis, namely *Ero1lb* and *Slc30a8*, are decreased, leading to fewer dense core granules[38,63]. In agreement with our findings, a decrease in mature insulin secretory granule number is similarly observed in Nkx6-1 knockout islets[11]. Collectively, the loss of these Med15-regulated genes

https://doi.org/10.1038/s41467-024-52801-9

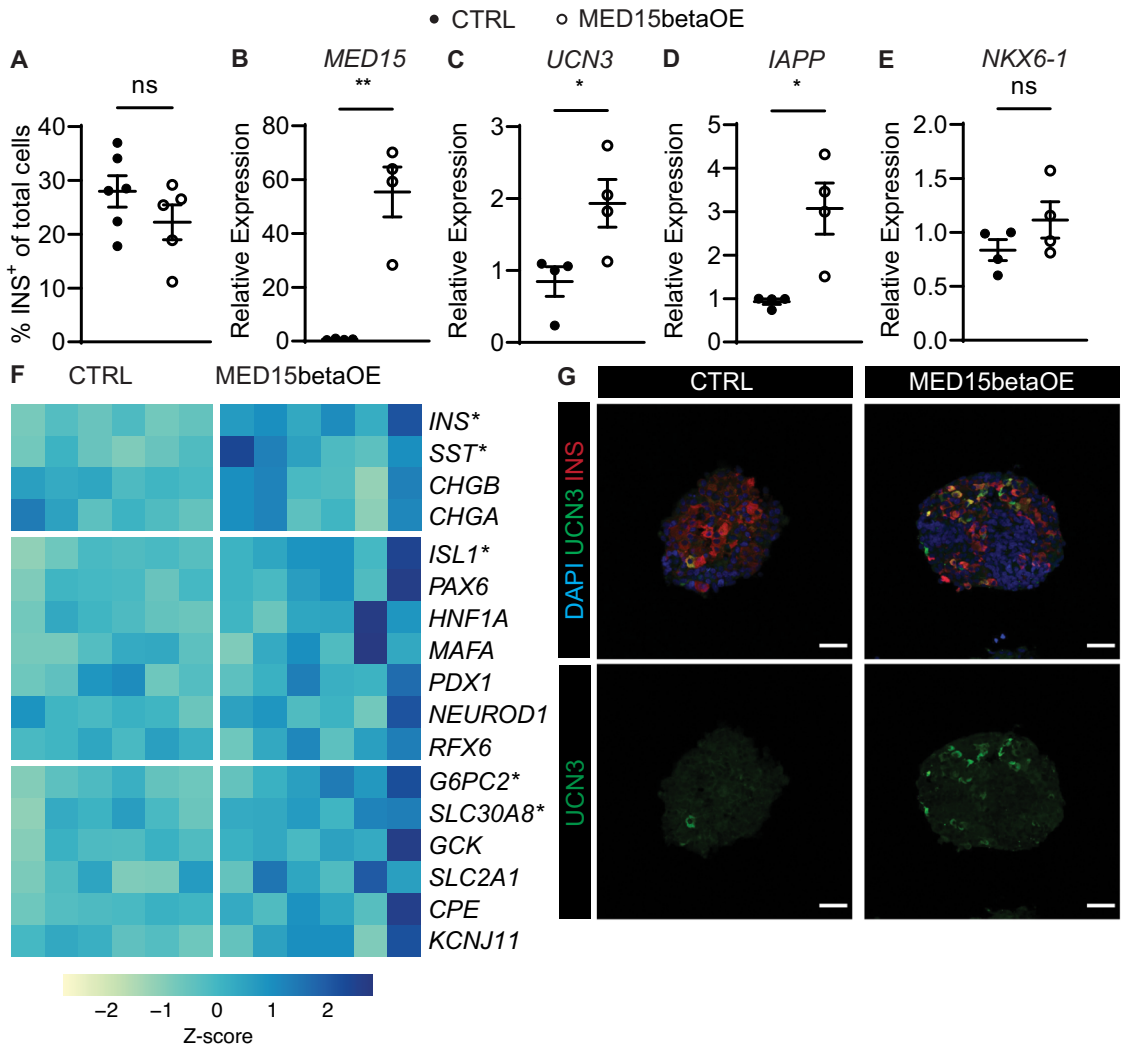

Fig. 6 | Overexpression of MED15 drives β-cell maturation marker expression in human embryonic stem cell (hESC)-derived pancreatic islets. A Differentiation efficiencies of Stage 6 Day 23–26 stem cell-derived spheroids derived from CTRL (closed circles; $n = 6$ differentiations) and MED15betaOE (open circles; $n = 5$ differentiations) hESC lines; error bars represent mean ± SEM. **B** *MED15*, **C** *UCN3*, **D** *IAPP*, and **E** *NKX6-1* transcript levels in Stage 6 Day 23–26 sorted INS-expressing differentiated islet cells derived from CTRL (closed circles) and MED15betaOE (open circles) hESCs ($n = 4$ differentiations); $^{*}p \le 0.05$; $^{**}p \le 0.005$ by two-tailed unpaired Student's *t*-test; error bars represent mean ± SEM. **F** Gene expression heatmap using NanoString profiling of sorted INS-expressing cells from Stage 6 Day 23–26 differentiated islets derived from CTRL and MED15betaOE hESCs, $n = 6$ differentiations, $^{*}p \le 0.05$ by two-tailed unpaired Student's *t*-test. **G** UCN3 (green) and INS (red) protein expression in Stage 6 Day 23 differentiated spheroids derived from CTRL and MED15betaOE hESC lines; blue = DAPI; representative of $n = 3$ differentiations; scale bars = 50 µm. Source data are provided as Source_Data.xlsx.

likely contributes to the impaired glucose tolerance observed in M15betaKO mice.

Mediator subunit interactions with transcription factor partners can selectively activate distinct gene regulatory networks in cell and developmental-specific manners[64,65]. Here, we show that Med15 physically interacts with Nkx6-1 and NeuroD1, but it may also bind other transcription factors at actively transcribed regions (Fig. 4F–H) to confer β-cell maturation. In contrast, Med1 did not bind Nkx6-1 in our assays, and Med1 and Med15-bound regions were often distinct (Fig. 4E, I). These results demonstrate that, in β-cells, individual Mediator subunit (e.g., Med15)::transcription factor interactions dictate how Mediator governs gene expression and cell-type specific functions.

As deletion of Med15 has a similar, yet distinct, phenotype to loss of Nkx6-1, it is likely that Med15 may have additional Nkx6-1 independent functions. For example, Mediator interacts with CTCF and the cohesin complex at intergenic boundaries to enable chromatin looping[66,67]. Such chromatin looping is important for pancreatic islet function and may be altered in T2D[68–70]. Additionally, Mediator is important for the formation of dense regions of enhancers known as super-enhancers[71]. Thus, future studies could determine if Med15, through its roles in Mediator, promotes enhancer-promoter looping or interactions at super-enhancers in order to drive the expression of genes required for β-cell maturation and to determine whether loss of these interactions predisposes to diabetes.

In our studies, immature hESC-derived insulin-producing cells genetically engineered to express high levels of MED15 had elevated expression of β-cell maturation markers. Of note, several of the genes upregulated in these human insulin-producing cells (*SLC30A8*, *IAPP*, *UCN3*, and *G6PC2*) were bound and regulated by Med15 in mouse islets, suggesting that these are conserved MED15 targets. However, it remains unclear how changing the amount of one Mediator subunit would affect the activity of the entire complex. We speculate that providing MED15 earlier following β-cell specification might improve maturation by increasing MED15 availability, turnover in the complex,

recruitment to enhancers by transcription factors, and stability of transcriptional machinery. Further investigation into stabilizing MED15 by reducing its degradation or into modulating specific MED15-transcription factor interactions pharmacologically, as done for the MED15–SREBP interaction, may prove useful in improving the maturation of stem cell-derived β-cells for the treatment of those with insulin-dependent diabetes[72,73].

Taken together, our work demonstrates the importance of Med15 and Mediator in the process of β-cell maturation, likely at least in part through mediating interactions between maturation transcription factor binding sites and core gene promoters. Further understanding how MED15 and Mediator regulate gene expression at regions that regulate β-cell maturation genes might allow for better in vitro production of β-cells with improved insulin secretion and understanding how its dysregulation could predispose to diabetes.

Methods

Animals and human islet studies

All mouse experiments were approved by the University of British Columbia Animal Care Committee. The Med15^{tm1a}(KOMP)Wtsi mouse JM8A1.N3 embryonic stem cells used for this research project were obtained from the trans-NIH Knock-Out Mouse Project (KOMP) and obtained from the KOMP Repository (www.komp.org) and injected into B6-Alb 8-cell stage embryos that were implanted into pseudo-pregnant C57BL/6J females (Mouse Animal Production Service, Centre for Molecular Medicine and Therapeutics). Germline transmission of founders was confirmed by genotyping.

Animals were housed under a 12-h light/dark cycle, fed ad libitum with a standard chow diet (5010; Lab Diets). Mouse strains used were on the C57BL/6J background. Throughout this study, males were studied unless otherwise stated. Control mice were littermate *Med15*$^{fl/fl}$; *Ins1*$^{+/+}$ or *Med15*$^{+/+}$; *Ins1*$^{Cre/+}$, whereas experimental mice were *Med15*$^{fl/fl}$; *Ins1*$^{Cre/+}$. Mice were euthanized following UBC SOP 009E4 by carbon dioxide followed by cervical dislocation. Human islet studies were approved by the BC Children's and Women's Hospital Research Ethics Board. Human islets for research were provided by Prodo Labs, the University of Alberta Clinical Islet Transplantation Program[74] or Alberta Diabetes Institute IsletCore at the University of Alberta in Edmonton (http://www.bcell.org/adi-isletcore.html) under written informed consent. The University of Alberta islet isolation facilities receive assistance from the Human Organ Procurement and Exchange (HOPE) program, Trillium Gift of Life Network (TGLN), and other Canadian organ procurement organizations. Islet isolation was approved by the Human Research Ethics Board at the University of Alberta (Pro00013094). All donors' families gave informed consent for the use of pancreatic tissue in research.

Gene expression analyses

Human islets were washed with 1xPBS and placed in RLT buffer (QIAGEN 79216) containing 1% β-mercaptoethanol (Sigma-Aldrich M6250), homogenized by vortexing, and hybridized to a custom CodeSet Plus chip. All probes are listed in Supplementary Data 3. CodeSet was then read on a Nanostring nCounter Sprint and analyzed using nSolver 3.0 for differential expression. Data was normalized by 6 housekeeping genes, including *B2M*, *GAPDH*, *GUSB*, *HPRT1*, *POLR2A*, and *TBP*. Significance was assessed by Student's *t*-test for each probe.

Quantitative PCR was carried out as previously described[75] using the following primers and probes labeled with FAM, ZEN, and Iowa Black FQ (IDT Technologies). *Med15* (Forward: GAC CAC CAT CGG AGC AC; Reverse: TCA AAA CCA ACC ACC ACA GA; Probe: CCA CAG TCA CAG AGC CAG CCT TT), *Med1* (Forward: CCA AAC AGC TGA CCA AAT GC; Reverse: CAG AAC AGA CCT TGG AGT GAA; Probe: ACC CTC TTC TCC ATT ACT TGA CGC AC), *Med14* (Forward: GCC TTC TGT GTT TCC TCA CTT; Reverse: TGG TCT TCG ATT GGA GTT GTC; Probe: AGC CAT CAC CTT CCA CTT GCA CT), *Med17* (Forward: CTT CTA ATT TTG TCT GCC AGT GTG; Reverse: TCT ATT CAG AAA CAG GCT CCA G; Probe: ACC TTT GCC /ZEN/CAA ATC CAA GCC AG), *Med23* (Forward: CAC TGG ATT TCG TAT GAG CCA; Reverse: ACT CCC TTA CCG ATG AAC CT; Probe: CAT GCC AAG ATG AGC CTT ATT CAC AGC), *MED15* (Forward: GAC CTG AGT AAG ATG AAG AGC C; Reverse: ACC GCC ATG TCA TTC TTG AG; Probe: TGT CCC CTG AAG ACC TTG CAA AAG T), *UCN3* (Forward: CTT GGC TTT GTA GAA CTT GTG G; Reverse: CCT CCC TGA GCG TTT CG; Probe: AAG TGG ACC GGC ATC AGC ATC T), *IAPP* (Forward: TGC TGA TAT TGC TGA CAT TGA AAC; Reverse: TCC GCT TTT CCA CCT GAT G; Probe: TGG GCA TCC TGA AGC TGC AAG TA), *NKX6-1* (Forward: TCG TTT GGC CTA TTC GTT GG; Reverse: TGT CTC CGA GTC CTG CTT C; Probe: TGC TTC TTC CTC CAC TTG GTC CG).

Intraperitoneal glucose tolerance test

Following a 10-h fast during the dark cycle, mice were weighed, and fasting saphenous vein blood glucose levels were obtained using a OneTouch UltraMini glucometer (Lifescan). Two grams per kilogram of 40% w/v D-glucose was delivered via intraperitoneal injection, and blood glucose levels were determined at 15, 30, 45, 60, and 90 min. Blood was collected at fasting and 10 min intraperitoneal glucose injection for determination of plasma insulin levels using ELISA (ALPCO STELLUX, 80-INSMR-CH10). Blood glucose levels greater than the glucometer detection limit are reported as 33.3 mM.

Insulin ELISA

A chemiluminescent ELISA kit (ALPCO STELLUX, 80-INSMR-CH10) was utilized according to the manufacturer's instructions. Serum insulin samples were used directly. GSIS basal samples were used directly; 16 mM glucose incubation media were diluted 5×, 40 mM KCl incubation media were diluted 20×, and acid ethanol total insulin samples were diluted 200×. Briefly, 5 µL per well of samples and standards were loaded in two technical replicates, with standards for each separate plate used. Samples were incubated for 2 h on an orbital shaker at 850 RPM with insulin-antibody conjugate, washed 6 times, and incubated with substrate for 1 min. ELISA plates were read on a POLARstar Omega microplate reader (BMG Labtech, Guelph, ON, Canada) with 1 s integration time per well.

Morphometric analysis and immunofluorescence

Sixteen sections (250-µm intervals) of each pancreas were imaged on a BX61 widefield fluorescence microscope and tiled using the cellSens Dimension software (Olympus). CellProfiler v2.1.1 was used to quantify images, and counts were normalized to total pancreatic nuclei[76]. For validation of RNA-seq targets, sections were imaged using confocal microscopy (Leica SP8; Leica Microsystems) and counted as above. All insulin-positive (INS$^+$) cells were normalized to the total number of DAPI$^+$ cells counted.

Perifusion and static incubation insulin secretion assays

Perifusion insulin secretion was performed using a Perifusion V2.0.0 system (Biorep). To assess GSIS, islets were first perifused with 2.8 mM glucose in Krebs-ringer bicarbonate HEPES (KRBH; 114 mM NaCl, 20 mM HEPES, 4.7 mM KCl, 2.5 mM $CaCl_2$, 1.2 mM KH_2PO_4, 1.2 mM $MgSO_4$, 0.2% BSA, pH 7.4) followed by 25 mM glucose; 10 mM α-ketoglutarate was used to bypass glucose uptake. Ten islets per well were removed to assess total insulin, removed, and transferred to 500 µL of acid ethanol (0.1 M HCl in 70% ethanol in H_2O) and stored O/N at −20 °C. The remaining islets were then lysed in RIPA buffer, and DNA concentration was measured using a Qubit fluorometer.

For static incubation, 1 day prior to experiments, 804G matrix was deposited onto 12-well flat-bottom tissue culture plates. On the day of experiment, 804G matrix-coated wells were washed 3 times with sterile water and allowed to briefly air-dry. Then, 1 mL of RPMI 1640

with 10% FBS (Gibco LS10082147), 100 U/mL penicillin, 100 µg/mL streptomycin, and 2 mM L-glutamine was aliquoted into each well. Islets were isolated, and 50 size-matched islets were deposited per well and allowed to recover overnight. On the following day, islets were washed in PBS and pre-incubated in 500 µL of KRBH supplemented with 2.8 mM D-glucose for 1 h. After preincubation, the media was exchanged with 500 µL KRBH with 2.8 mM D-glucose and incubated again for 1 h for basal secreted insulin levels, and replaced with KRBH supplemented with 16 mM D-glucose or 40 mM KCl for 1 h for stimulated insulin levels. Finally, 10 islets per well were removed to assess total insulin, transferred to 500 µL of acid ethanol (0.1 M HCl in 70% ethanol in H_2O), and stored at −20 °C. Remaining islets were washed with PBS, and cell lysate was collected for protein quantification.

Transcriptome analysis by RNA sequencing

Following total RNA extraction and DNase treatment[77], samples were rRNA depleted using a RiboGone™ Mammalian-Low Input Ribosomal RNA Removal Kit (Takara Bio USA 634847), Agencourt AMPure XP SPRI beads (Beckman Coulter A63881), and DynaMag-96 side magnet (ThermoFisher Scientific 12331D). rRNA-depleted RNA samples were assessed for rRNA depletion, RNA integrity, size distribution, and concentration prior to library generation with the Agilent RNA Pico 6000 kit on an Agilent 2100 Bioanalyzer (Agilent Technologies 5067-1511). rRNA-depleted RNA passing quality control was used in the SMARTer Stranded RNA-seq Kit (Takara Bio USA 634839). Following RNA incubation with stranded N6 primer, buffer, and water, samples were incubated at 94 °C for 4 min, appropriate for samples with RIN values between 4–7. Following purification of first-strand cDNA, libraries were PCR amplified in accordance with their input RNA amount, and purified. Final adapter-ligated cDNAs were quantified by Qubit® 3.0 dsDNA high-sensitivity assay kit (ThermoFisher Scientific Q32854) together with qPCR amplification using standard curves of a known concentration of adapter-ligated libraries. Sequencing was performed on the NextSeq 500 (Illumina, San Diego, CA, USA) with the High Output Reagent Cartridge v2 150 cycles (75 bp × 2).

Bioinformatics analysis

Linux Ubuntu operating system version 14.04 LTS was used for analyses. Fastq files from each sample were concatenated. ENSEMBL Mus musculus genome GRCm38p.4 fastq and gtf annotation file were used for alignments. STAR v2.4.0.1[78] was used to index the genome fastq files, align sample transcriptomes against the genome, and output as sorted by coordinate BAM files. Counts were generated from BAM files with HTSeq[79] against annotated genes from GRCm38p.4. Differential gene analysis was performed between control and experimental samples using DESeq2[80], with an FPKM criteria of ≥5 in two or more samples, applying a Wald test on *p*-values from genes passing filtering, and adjusted for multiple testing via Benjamini and Hochberg procedure. Gene set enrichment analyses were performed with fgsea version 1.30.0[81].

Electron microscopy and insulin secretory granule quantification

Freshly isolated islets were placed in 2% fresh glutaraldehyde in PBS and prepared for transmission electron microscopy using a JEOL 1200EX TEMSCAN transmission electron microscope. For insulin secretory granule quantification, approximately 15–20 β-cells per genotype were analyzed on 10 random planes at 3000×. CellProfiler 3.0.0 was used to quantify granule counts and the size of halo around dense cores[76].

Mitochondrial activity and 3D morphology measurements

Islets were washed with Minimum Essential Media (MEM, Corning #15-015-CV), dispersed with 0.05% trypsin, and seeded on 804G coated coverslips. The following day, the cells were pre-incubated 1 h with 2.8 mM glucose in KRBH. This was followed by 1.5 h incubation in 2.8 mM glucose, 18 mM glucose or 2.8 mM glucose + 10 mM α-ketoglutarate, with fluorescent 25 nM tetramethylrhodamine ethyl ester (TMRE) (Sigma-Aldrich 87917), 50 nM mitotracker green FM (MTG) (ThermoFisher M7514) and 0.1 µg/mL Hoechst (ThermoFisher H3570) added the final 30 min. Cells were imaged in a Tokai Hit INUBTFP-WSKM stage-top incubator at 37 °C on a Leica SP8 Confocal Microscope (Concord, Ontario) using a 63XHC Plan Apochromatic water immersion objective (NA = 1.2). For 3D analysis, image stacks were acquired with z-spacing set to optimal Nyquist sampling parameters and deconvolved using Huygens Professional software (Scientific Volume Imaging, Netherlands). Mitochondrial morphological and functional features were extracted and quantified in ImageJ/Fiji using a mitochondria analyzer pipeline and plugin developed in-house[82]. Briefly, images were processed using the ImageJ Subtract Background and Sigma Filer Plus modules, and mitochondria were then identified using a local Weighted Mean-based threshold algorithm. 2D morphological descriptors were extracted from the resulting binary image using the Analyze Particles command, while 3D features were quantified using a combination of the 3D Object Counter and Particle Analyzer 3D commands (part of the MorphoLibJ package)[83].

Seahorse mitochondrial function assay

Seahorse assay was performed as previously described[84]. In brief, Seahorse XFe96 spheroid microplates (Agilent, 102959-100) were coated with CellTak (ThermoFisher, C354240) according to the manufacturer's instructions. The following day, 10 size-matched islets in 15 µL of RPMI 1640 supplemented with 10% FBS, 100 U/mL penicillin, 100 µg/mL streptomycin, and 2 mM L-glutamine were gently deposited into the center of the spheroid wells with a canted P20 pipette tip. Islets attached overnight, with 6 technical replicates per animal, and 4 wells left as blanks with 175 µL prepared RPMI. The Seahorse sensor plate was prepared by adding 200 µL of buffer calibrant to the buffer cartridge. Sensor cartridge was placed into the buffer, mixed gently several times and placed into a 37 °C non-CO_2 incubator overnight. Seahorse media was prepared fresh: Gibco D5030 with 2.8 mM glucose, 2 mM Glutamine, pH 7.4, and filter sterilized. Islets were washed by removing 150 µL of media with a multichannel pipette, working in groups. Seahorse media (175 µL) was replaced, removed again, and 150 µL of Seahorse media was added back for a final volume of 175 µL. Islets were incubated at 37 °C in a non-CO_2 incubator for at least 1 h. Drugs were prepared in Seahorse media during this time as follows: 16 mM Glucose, FCCP (# 15218), Oligomycin Complex (# 11341), and antimycin A (# 2247) + Rotenone (# 13995) (Cayman Chemical Company; Ann Arbor, MI, USA). The Seahorse machine was run with the following measurement cycles: 5 cycles basal Seahorse media, 6 cycles 16 mM glucose, 4 cycles of oligomycin, 4 cycles of FCCP, 4 cycles of AA + Rotenone. Following measurements, islet images were captured on an Olympus inverted microscope and quantified for image area on ImagePro Analyzer (Mediacy, Rockville, MD, USA). Readings were then normalized to islet area.

Glucose uptake assay

Glucose uptake assay was performed as described[85]. In brief, islets were dispersed with trypsin and seeded on an 804 G coated coverslip. The following day, 2.8 mM glucose in KRBH was used to pre-incubate islet cells followed by 200 µM 2-[N-(7-nitrobenz-2-oxa-1, 3-diazol-4-yl) amino]-2deoxy-D-glucose (2-NBDG) for 10 min. Dispersed cells were imaged using confocal microscopy (Leica SP8; Leica Microsystems), and intracellular fluorescence was quantified with ImageJ software.

Chromatin immunoprecipitation sequencing and analysis

Chromatin was isolated from MIN6 cells and fragmented using an M220 focused ultrasonicator with milliTUBE 1 mL with AFA fiber (Covaris, 520130), and chromatin immunoprecipitation was carried

out as described using MED15 (11566-AP; ProteinTech)[86] or Med1[87] (A300-793A; Bethyl) antibodies. ChIP-seq libraries were constructed using a ThruPLEX DNA-seq Kit (R400427; Clontech). Libraries were sequenced on an Illumina NextSeq500 at 2x76bp.

Sequenced reads were quality trimmed using Trimmomatic v0.39[88] using flags '2:30:10:2:True LEADING:3 TRAILING:3 SLIDINGWINDOW:4:20 MINLEN:35'. Trimmed reads were aligned to the mm10 genome using Bowtie2 v2.4.4[89] with flags '--very-sensitive --no-unal --no-discordant'. Aligned reads with mapping quality score <30, duplicate reads, reads that mapped to chromosomes X, Y, or M, and reads that mapped to annotated high-background regions[90] were removed. Peaks were called using MACS3 v3.0.0a7[91] with flags '-f BAM -g mm -B -q 0.01'. Genome tracks were created by converting reads to bigwig file format (scaled to reads per million mapped reads) using BEDtools v2.26.0[92] genomecov and bedGraphToBigWig and visualizing in the Integrative Genomics Viewer[93]. Heatmaps were generated using deepTools v3.5.1[94]. DNA motif analysis was performed using HOMER v4.11.1 findMotifsGenome with flags '-size 200 -mask' and using the union of all Med1 and Med15 peaks as background. For the analyses using published transcription factor ChIP-seq data, bigwig files and BED files of peak locations were downloaded from the Cistrome data browser[95]. For the analyses using promoters and enhancers, promoter locations are the 5′ end of the Ensembl Canonical transcript ± 5 kb of genes detected in our RNA-seq data, and enhancers are FANTOM5 high-confidence CAGE-seq peak enhancer annotations[96].

Co-immunoprecipitation and in vitro interaction studies

Co-immunoprecipitation (CoIP) was carried out as described using MED15 antibody[84]. In brief, MIN6 cells were harvested with CoIP lysis buffer (150 mM NaCl, 20 mM Tris pH 7.4, 1 mM EDTA, 0.5 mM EGTA, 5% glycerol, 0.5% NP-40, 1 mM Na_3VO_4, 50 mM NaF, 50 mM β-glycerophosphate, 1x Roche protease inhibitor), insoluble material spun down, and supernatant collected. Protein concentration was determined via BCA assay (ThermoFisher, 23225), 10% of each lysate was set aside as input, and 2 μg antibody added to 300 μg lysate. Tubes were rotated overnight at 4 °C, 2 mg of magnetic Dynabeads were added, and bead-antigen-antibody complexes were washed 3 times with CoIP lysis buffer and separated. Then, 1% SDS was added to beads in CoIP lysis buffer, boiled for 10 min, and Western blot performed for target proteins.

In vitro interaction studies were performed with tagged proteins expressed by recombinant plasmids. To construct pCMV-mMed15-Flag-CT, primers 5′AATTGAATTCATGGACGTTTCGGGGCAGGAG and 5′TTAAGTCGACGGGAGCTGCAGCAGCCTTGA were used to amplify DNA fragment from mouse islet cDNAs. The PCR fragment was then digested with EcoR I and Sal I, and cloned into EcoR I and Sal I linearized pCMV-Flag-CT. To construct pcDNA3.1-HA-mNKX6.1, primers 5′ AATTGAATTCATGGAGTACCCATACGACGTACCA and 5′ TTAACTCGAGTCAGGACGAGCCCTCGGCCTC were used to amply HA-mNKX6.1 fragment from plasmid pGADT7-newMCS-HA-mNKX6.1 that was generated by cloning mNKX6.1 cDNA into pGADT7-newMCS with Nde I and Xho I. The PCR fragment was digested with EcoR I and Xho I and cloned into EcoR I and Xho I linearized pcDNA3.1. All constructs were confirmed by DNA sequencing. Then, HA-mNKX6.1 was expressed in 293T cells and purified with Pierce Anti-HA agarose (ThermoFisher cat#26181) and eluted with HA Synthetic Peptide (ThermoFisher Cat# 26184) according to the manufacturer's protocol. mMED15-FLAG or Ctrl-FLAG was expressed in 293T cells and immobilized on Pierce anti-Flag affinity resin (ThermoFisher cat#36801), which was followed by incubation with purified HA-mNKX6.1 eluted with HA peptide. Incubation was done at 4 °C overnight, which was followed by washing 6 times at 20 mMTris buffer pH 7.5 150 mM NaCl containing 0.5% NP-40. Bound HA-mNKX6.1 was examined by Western blot.

Alphafold and Alphapulldown

The multiple sequence alignment (MSA) and template features were generated through the AlphaFold/HHBlits databases[51]. Subsequent structure prediction was performed with MED15 (uniprot: Q96RN5) against each gene in Fig. S8A (baits, candidates as described)[52]. Figures 5 and S7 display the highest likelihood interaction for each relationship. The table in Fig. S7A provides quality and likelihood metrics (IPTM, PI_score, mpDockQ) calculated by AlphaPulldown, for the validity of the reported interface interaction. IPTM, interface protein TM scores range 0–1, with values >0.85 reliable to be defined as high-confidence PPI models[97]. pDockQ scores developed by Bryant et al.[98] should be >0.23 for acceptable quality of the protein interface. PI scores, developed by Malhotra et al.[99], are binary classifiers with positive values corresponding to native-like structures. PI score calculation produces additional metrics, such as contact pairs and hydrogen bonds, relating to the number of each interaction at less than seven Angstroms between interfaces and is helpful in understanding the predicted interface.

CRISPR knock-in and hESC differentiation

The CRISPR/Cas9 system was used to generate MED15βOE hESC line as previously described using pCCC to express gRNA (5′-TGCAACTAGACGCAG CCCGC-3′) and Cas9[53]. Electroporation, selection, picking, and expansion of clones was previously described[53] with the following changes: StemFlex Medium (Gibco) was used for clonal expansion and cell culture, and the following primers were used for genotyping across the homology arms: LL688, TGACCGCAGATTCAAGTGTT; LL814, GTCAGGCTCTGGAGTGCATT; LL789, GAAGGATTGGAGCTACGGGG; LL790, AGCTCATGGTGCCATCTGAC. Positive clones were subjected to Sanger sequencing to confirm fidelity of recombination and tested for chromosomal abnormalities using the hPSC Genetic Analysis Kit and the manufacturer's instructions (STEMCELL Technologies #07550). Genetically modified hESCs were differentiated as spheroids as recently described[54,55].

Data analyses

Measurements were performed on independent samples unless otherwise specified, with one biological replicate being defined as one mouse, one cell passage or one stem cell differentiation. Sex-specific analyses were carried out for many mouse studies, as noted in the figures; human islets gene expression studies were not segregated or analyzed by sex, although age, sex and BMI of the organ donors may be found in Supplementary Data S1. The majority of experimental approaches included technical replicates, and these were typically averaged and reported as 1 biological replicate unless otherwise noted. Throughout, we report results from at least 3 biological replicates. Statistical analyses were performed using Prism 9.0 (GraphPad Software, La Jolla, CA) or R version 4.2.3. Statistical significance was determined using parametric (Student's *t*-test or ANOVA) or non-parametric (Mann–Whitney *U*-test or Kruskal–Wallis), permutation, or Fisher exact tests with appropriate post-hoc tests, as noted in figure legends. Unless otherwise noted in figure legends, a p-value <0.05 was considered to indicate a statistically significant difference (*) between groups. Data are presented as the mean ± SEM.

Reporting summary

Further information on research design is available in the Nature Portfolio Reporting Summary linked to this article.

Data availability

All data supporting the findings described in this manuscript are available in the article and in the Supplementary Information and from the corresponding author upon request. The sequencing data generated in this study have been deposited in the NCBI Gene Expression Omnibus database under accession # GSE137145. The Nanostring gene

expression and processed RNAseq expression profiling data generated in this study are provided in the Supplementary Information/Source Data file. Other published datasets used in this work include GSE30298, GSE84759, GSE40975, GSE62844, GSE59622, GSE122120, GSE84759, GSE79785. Source data are provided with this paper.

References

1. Blum, B. et al. Functional beta-cell maturation is marked by an increased glucose threshold and by expression of urocortin 3. *Nat. Biotechnol.* **30**, 261–264 (2012).
2. Barsby, T. & Otonkoski, T. Maturation of beta cells: lessons from in vivo and in vitro models. *Diabetologia* **65**, 917–930 (2022).
3. Kolic, J. et al. Proteomic predictors of individualized nutrient-specific insulin secretion in health and disease. *Cell Metab.* **36**, 1619–1633.e5 (2024).
4. Goodyer, W. R. et al. Neonatal β cell development in mice and humans is regulated by calcineurin/NFAT. *Dev. Cell* **23**, 21–34 (2012).
5. Heit, J. J., Karnik, S. K. & Kim, S. K. Intrinsic regulators of pancreatic beta-cell proliferation. *Annu. Rev. Cell Dev. Biol.* **22**, 311–338 (2006).
6. van der Meulen, T. et al. Urocortin3 mediates somatostatin-dependent negative feedback control of insulin secretion. *Nat. Med.* **21**, 769–776 (2015).
7. Balboa, D. et al. Functional, metabolic and transcriptional maturation of human pancreatic islets derived from stem cells. *Nat. Biotechnol.* **40**, 1042–1055 (2022).
8. Gu, C. et al. Pancreatic beta cells require NeuroD to achieve and maintain functional maturity. *Cell Metab.* **11**, 298–310 (2010).
9. Hang, Y. et al. The MafA transcription factor becomes essential to islet β-cells soon after birth. *Diabetes* **63**, 1994–2005 (2014).
10. Oliver-Krasinski, J. M. et al. The diabetes gene Pdx1 regulates the transcriptional network of pancreatic endocrine progenitor cells in mice. *J. Clin. Invest.* **119**, 1888–1898 (2009).
11. Taylor, B. L., Liu, F.-F. & Sander, M. Nkx6.1 is essential for maintaining the functional state of pancreatic beta cells. *Cell Rep.* **4**, 1262–1275 (2013).
12. Nishimura, W., Takahashi, S. & Yasuda, K. MafA is critical for maintenance of the mature beta cell phenotype in mice. *Diabetologia* **58**, 566–574 (2015).
13. Stolovich-Rain, M. et al. Weaning triggers a maturation step of pancreatic β cells. *Dev. Cell* **32**, 535–545 (2015).
14. Bevacqua, R. J. et al. SIX2 and SIX3 coordinately regulate functional maturity and fate of human pancreatic β cells. *Genes Dev.* **35**, 234–249 (2021).
15. Schwitzgebel, V. M. Many faces of monogenic diabetes. *J. Diab. Invest.* **5**, 121–133 (2014).
16. Poss, Z. C., Ebmeier, C. C. & Taatjes, D. J. The Mediator complex and transcription regulation. *Crit. Rev. Biochem. Mol. Biol.* **48**, 575–608 (2013).
17. Harper, T. M. & Taatjes, D. J. The complex structure and function of Mediator. *J. Biol. Chem.* **293**, 13778–13785 (2018).
18. Soutourina, J. Transcription regulation by the Mediator complex. *Nat. Rev. Mol. Cell Biol.* **19**, 262–274 (2017).
19. Tsai, K.-L. et al. Mediator structure and rearrangements required for holoenzyme formation. *Nature* **544**, 196–201 (2017).
20. Verger, A., Monté, D. & Villeret, V. Twenty years of Mediator complex structural studies. *Biochem. Soc. Trans.* **47**, 399–410 (2019).
21. Haberle, V. et al. Transcriptional cofactors display specificity for distinct types of core promoters. *Nature* **570**, 122–126 (2019).
22. Taatjes, D. J. The human Mediator complex: a versatile, genome-wide regulator of transcription. *Trends Biochem. Sci.* **35**, 315–322 (2010).
23. Allen, B. L. & Taatjes, D. J. The Mediator complex: a central integrator of transcription. *Nat. Rev. Mol. Cell Biol.* **16**, 155–166 (2015).
24. Tsai, K.-L. et al. Subunit architecture and functional modular rearrangements of the transcriptional mediator complex. *Cell* **157**, 1430–1444 (2014).
25. Plaschka, C. et al. Architecture of the RNA polymerase II-Mediator core initiation complex. *Nature* **518**, 376–380 (2015).
26. Ansari, S. A. & Morse, R. H. Mechanisms of Mediator complex action in transcriptional activation. *Cell. Mol. Life Sci.* **70**, 2743–2756 (2013).
27. Kemmeren, P. et al. Large-scale genetic perturbations reveal regulatory networks and an abundance of gene-specific repressors. *Cell* **157**, 740–752 (2014).
28. Yang, F. et al. An ARC/Mediator subunit required for SREBP control of cholesterol and lipid homeostasis. *Nature* **442**, 700–704 (2006).
29. Lee, D. et al. SREBP and MDT-15 protect *C. elegans* from glucose-induced accelerated aging by preventing accumulation of saturated fat. *Genes Dev.* **29**, 2490–2503 (2015).
30. Goh, G. Y. S. et al. The conserved Mediator subunit MDT-15 is required for oxidative stress responses in *Caenorhabditis elegans*. *Aging Cell* **13**, 70–79 (2014).
31. Goh, G. Y. S. et al. NHR-49/HNF4 integrates regulation of fatty acid metabolism with a protective transcriptional response to oxidative stress and fasting. *Aging Cell* **17**, e12743 (2018).
32. Vozdek, R., Long, Y. & Ma, D. K. The receptor tyrosine kinase HIR-1 coordinates HIF-independent responses to hypoxia and extracellular matrix injury. *Sci. Signal* **11**, eaat0138 (2018).
33. Shomer, N. et al. Mediator subunit MDT-15/MED15 and Nuclear Receptor HIZR-1/HNF4 cooperate to regulate toxic metal stress responses in *Caenorhabditis elegans*. *PLoS Genet.* **15**, e1008508 (2019).
34. Park, Y. J. & Woo, M. Pancreatic β cells: gatekeepers of type 2 diabetes. *J. Cell Biol.* **218**, 1094–1095 (2019).
35. Gerber, P. A. & Rutter, G. A. The role of oxidative stress and hypoxia in pancreatic beta-cell dysfunction in diabetes mellitus. *Antioxid. Redox Signal.* **26**, 501–518 (2017).
36. Nyengaard, J. R., Ido, Y., Kilo, C. & Williamson, J. R. Interactions between hyperglycemia and hypoxia: implications for diabetic retinopathy. *Diabetes* **53**, 2931–2938 (2004).
37. Thorens, B. et al. *Ins1*^{Cre} knock-in mice for beta cell-specific gene recombination. *Diabetologia* **58**, 558–565 (2015).
38. Zito, E., Chin, K.-T., Blais, J., Harding, H. P. & Ron, D. ERO1-β, a pancreas-specific disulfide oxidase, promotes insulin biogenesis and glucose homeostasis. *J. Cell Biol.* **188**, 821–832 (2010).
39. Guillam, M. T., Dupraz, P. & Thorens, B. Glucose uptake, utilization, and signaling in GLUT2-null islets. *Diabetes* **49**, 1485–1491 (2000).
40. Jaafar, R. et al. mTORC1-to-AMPK switching underlies β cell metabolic plasticity during maturation and diabetes. *J. Clin. Invest.* **129**, 4124–4137 (2019).
41. Helman, A. et al. A Nutrient-Sensing Transition at Birth Triggers Glucose-Responsive Insulin Secretion. *Cell Metab.* **31**, 1004–1006 (2020).
42. Eguchi, K. & Nagai, R. Islet inflammation in type 2 diabetes and physiology. *J. Clin. Invest.* **127**, 14–23 (2017).
43. Apaolaza, P. S. et al. Islet expression of type I interferon response sensors is associated with immune infiltration and viral infection in type 1 diabetes. *Sci. Adv.* **7**, eabd6527 (2021).
44. Ito, M., Yuan, C.-X., Okano, H. J., Darnell, R. B. & Roeder, R. G. Involvement of the TRAP220 component of the TRAP/SMCC coactivator complex in embryonic development and thyroid hormone action. *Mol. Cell* **5**, 683–693 (2000).
45. Grants, J. M., Goh, G. Y. S. & Taubert, S. The Mediator complex of *Caenorhabditis elegans*: insights into the developmental and physiological roles of a conserved transcriptional coregulator. *Nucleic Acids Res.* **43**, 2442–2453 (2015).
46. Romer, A. I., Singer, R. A., Sui, L., Egli, D. & Sussel, L. Murine perinatal β-cell proliferation and the differentiation of human stem

cell–derived insulin-expressing cells require NEUROD1. *Diabetes* **68**, 2259–2271 (2019).
47. Gao, N. et al. Foxa2 controls vesicle docking and insulin secretion in mature Beta cells. *Cell Metab.* **6**, 267–279 (2007).
48. Ediger, B. N. et al. LIM domain–binding 1 maintains the terminally differentiated state of pancreatic β cells. *J. Clin. Invest.* **127**, 215–229 (2017).
49. Piccand, J. et al. Rfx6 maintains the functional identity of adult pancreatic β cells. *Cell Rep.* **9**, 2219–2232 (2014).
50. Scoville, D. W., Lichti-Kaiser, K., Grimm, S. A. & Jetten, A. M. GLIS3 binds pancreatic beta cell regulatory regions alongside other islet transcription factors. *J. Endocrinol.* **243**, 1–14 (2019).
51. Jumper, J. et al. Highly accurate protein structure prediction with AlphaFold. *Nature* **596**, 583–589 (2021).
52. Yu, D., Chojnowski, G., Rosenthal, M. & Kosinski, J. AlphaPulldown—a Python package for protein–protein interaction screens using AlphaFold-Multimer. *Bioinformatics* **39**, btac749 (2023).
53. Krentz, N. A. J., Nian, C. & Lynn, F. C. TALEN/CRISPR-mediated eGFP knock-in add-on at the OCT4 locus does not impact differentiation of human embryonic stem cells towards endoderm. *PLoS ONE* **9**, e114275 (2014).
54. Novakovsky, G. et al. In silico discovery of small molecules for efficient stem cell differentiation into definitive endoderm. *Stem Cell Rep.* **18**, 765–781 (2023).
55. Mar, S. et al. Tracking insulin- and glucagon-expressing bihormonal cells during differentiation using an *INSULIN* and *GLUCAGON* double reporter human embryonic stem cell line. Preprint at *bioRxiv* https://doi.org/10.1101/2023.04.19.537542 (2023).
56. Castro-Gutierrez, R., Alkanani, A., Mathews, C. E., Michels, A. & Russ, H. A. Protecting stem cell derived pancreatic beta-like cells from diabetogenic T cell recognition. *Front. Endocrinol.* **12**, 707881 (2021).
57. Bastidas-Ponce, A., Scheibner, K., Lickert, H. & Bakhti, M. Cellular and molecular mechanisms coordinating pancreas development. *Development* **144**, 2873–2888 (2017).
58. Conrad, E., Stein, R. & Hunter, C. S. Revealing transcription factors during human pancreatic β cell development. *Trends Endocrinol. Metab.* **25**, 407–414 (2014).
59. Sabatini, P. V. & Lynn, F. C. All-encomPASsing regulation of β-cells: PAS domain proteins in β-cell dysfunction and diabetes. *Trends Endocrinol. Metab.* **26**, 49–57 (2015).
60. Jennings, R. E., Berry, A. A., Strutt, J. P., Gerrard, D. T. & Hanley, N. A. Human pancreas development. *Development* **142**, 3126–3137 (2015).
61. Yoshihara, E. et al. ERRγ is required for the metabolic maturation of therapeutically functional glucose-responsive β cells. *Cell Metab.* **23**, 622–634 (2016).
62. Špaček, T. et al. Nkx6.1 decline accompanies mitochondrial DNA reduction but subtle nucleoid size decrease in pancreatic islet β-cells of diabetic Goto Kakizaki rats. *Sci. Rep.* **7**, 15674 (2017).
63. Wijesekara, N. et al. Beta cell-specific Znt8 deletion in mice causes marked defects in insulin processing, crystallisation and secretion. *Diabetologia* **53**, 1656–1668 (2010).
64. Yin, J. W. & Wang, G. The Mediator complex: a master coordinator of transcription and cell lineage development. *Development* **141**, 977–987 (2014).
65. Ilchuk, L. A. et al. Genetically engineered mice unveil in vivo roles of the Mediator complex. *Int. J. Mol. Sci.* **24**, 9330 (2023).
66. Chereji, R. V. et al. Mediator binds to boundaries of chromosomal interaction domains and to proteins involved in DNA looping, RNA metabolism, chromatin remodeling, and actin assembly. *Nucleic Acids Res.* **45**, 8806–8821 (2017).
67. Kagey, M. H. et al. Mediator and cohesin connect gene expression and chromatin architecture. *Nature* **467**, 430–435 (2010).
68. Mishra, A. & Hawkins, R. D. Three-dimensional genome architecture and emerging technologies: looping in disease. *Genome Med.* **9**, 87 (2017).
69. Pasquali, L. et al. Pancreatic islet enhancer clusters enriched in type 2 diabetes risk-associated variants. *Nat. Genet.* **46**, 136–143 (2014).
70. Thurner, M. et al. Integration of human pancreatic islet genomic data refines regulatory mechanisms at Type 2 diabetes susceptibility loci. *eLife* **7**, e31977 (2018).
71. Whyte, W. A. et al. Master transcription factors and mediator establish super-enhancers at key cell identity genes. *Cell* **153**, 307–319 (2013).
72. Zhao, X. et al. Inhibition of SREBP transcriptional activity by a boron-containing compound improves lipid homeostasis in diet-induced obesity. *Diabetes* **63**, 2464–2473 (2014).
73. Ishikawa, H., Tachikawa, H., Miura, Y. & Takahashi, N. TRIM11 binds to and destabilizes a key component of the activator-mediated cofactor complex (ARC105) through the ubiquitin–proteasome system. *FEBS Lett.* **580**, 4784–4792 (2006).
74. Kin, T. et al. Contribution of a Single Islet Transplant Program to Basic Researchers in North America, Europe, and Asia through Distributing Human Islets. *OBM Transplant.* **8**, 212 (2024).
75. Xu, E. E., Sasaki, S., Speckmann, T., Nian, C. & Lynn, F. C. SOX4 allows facultative β-cell proliferation through repression of Cdkn1a. *Diabetes* **66**, 2213–2219 (2017).
76. Carpenter, A. E. et al. CellProfiler: image analysis software for identifying and quantifying cell phenotypes. *Genome Biol.* **7**, R100 (2006).
77. Xu, E. E. et al. SOX4 cooperates with neurogenin 3 to regulate endocrine pancreas formation in mouse models. *Diabetologia* **58**, 1013–1023 (2015).
78. Dobin, A. et al. STAR: ultrafast universal RNA-seq aligner. *Bioinformatics* **29**, 15–21 (2013).
79. Anders, S., Pyl, P. T. & Huber, W. HTSeq—a Python framework to work with high-throughput sequencing data. *Bioinformatics* **31**, 166–169 (2015).
80. Love, M. I., Huber, W. & Anders, S. Moderated estimation of fold change and dispersion for RNA-seq data with DESeq2. *Genome Biol.* **15**, 550 (2014).
81. Sergushichev, A. A. An algorithm for fast preranked gene set enrichment analysis using cumulative statistic calculation. Preprint at *bioRxiv* https://doi.org/10.1101/060012 (2016).
82. Chaudhry, A., Shi, R. & Luciani, D. S. A pipeline for multidimensional confocal analysis of mitochondrial morphology, function, and dynamics in pancreatic β-cells. *Am. J. Physiol. Endocrinol. Metab.* **318**, E87–E101 (2020).
83. Legland, D., Arganda-Carreras, I. & Andrey, P. MorphoLibJ: integrated library and plugins for mathematical morphology with ImageJ. *Bioinformatics* **32**, 3532–3534 (2016).
84. Sabatini, P. V. et al. Neuronal PAS domain protein 4 suppression of oxygen sensing optimizes metabolism during excitation of neuroendocrine cells. *Cell Rep.* **22**, 163–174 (2018).
85. Yamada, K. et al. Measurement of glucose uptake and intracellular calcium concentration in single, living pancreatic β-cells. *J. Biol. Chem.* **275**, 22278–22283 (2000).
86. Johnson, D. S., Mortazavi, A., Myers, R. M. & Wold, B. Genome-wide mapping of in vivo protein-DNA interactions. *Science* **316**, 1497–1502 (2007).
87. Harms, M. J. et al. PRDM16 binds MED1 and controls chromatin architecture to determine a brown fat transcriptional program. *Genes Dev.* **29**, 298–307 (2015).
88. Bolger, A. M., Lohse, M. & Usadel, B. Trimmomatic: a flexible trimmer for Illumina sequence data. *Bioinformatics* **30**, 2114–2120 (2014).
89. Langmead, B. & Salzberg, S. L. Fast gapped-read alignment with Bowtie 2. *Nat. Methods* **9**, 357–359 (2012).

90. Amemiya, H. M., Kundaje, A. & Boyle, A. P. The ENCODE blacklist: identification of problematic regions of the genome. *Sci. Rep.* **9**, 9354 (2019).
91. Zhang, Y. et al. Model-based analysis of ChIP-Seq (MACS). *Genome Biol.* **9**, R137 (2008).
92. Quinlan, A. R. & Hall, I. M. BEDTools: a flexible suite of utilities for comparing genomic features. *Bioinformatics* **26**, 841–842 (2010).
93. Robinson, J. T. et al. Integrative genomics viewer. *Nat. Biotechnol.* **29**, 24–26 (2011).
94. Ramírez, F., Dündar, F., Diehl, S., Grüning, B. A. & Manke, T. deepTools: a flexible platform for exploring deep-sequencing data. *Nucleic Acids Res.* **42**, W187–W191 (2014).
95. Mei, S. et al. Cistrome Data Browser: a data portal for ChIP-Seq and chromatin accessibility data in human and mouse. *Nucleic Acids Res.* **45**, D658–D662 (2017).
96. Arner, E. et al. Transcribed enhancers lead waves of coordinated transcription in transitioning mammalian cells. *Science* **347**, 1010–1014 (2015).
97. O'Reilly, F. J. et al. Protein complexes in cells by AI-assisted structural proteomics. *Mol. Syst. Biol.* **19**, e11544 (2023).
98. Bryant, P. MoLPC. GitLab https://gitlab.com/patrickbryant1/molpc (2022).
99. Malhotra, S. ppi_scoring. GitLab https://gitlab.com/sm2185/ppi_scoring/-/wikis/home (2021).

Acknowledgements

We thank Michelle Wang for helping breed the initial Med15$^{fl/fl}$ mice, Helena Winata for bioinformatic support, and Michelle Ying Ya Lee for help with data analysis. Operating grant support was from the Canadian Institutes of Health Research (CIHR; PJT-153199 and PJT-165988 to S.T.), Diabetes Canada (OG-3-15-4946-FL to F.C.L. and S.T.) and the JDRF (1-INO-2017-448-A-N to F.C.L.). Research infrastructure was funded by the Canada Foundation for Innovation (#33644). We are grateful to David Ron for providing rabbit anti ERO1LB antibody and Marc Huising for providing rabbit anti Ucn3 antibody. A.Z.K. was supported by a BC Children's Hospital Research Institute (BCCHR) Canucks for Kids Diabetes Research Laboratories scholarship, R.J.S. by NSERC CREATE, UBC, and CIHR CGS-D scholarships, S.T. by salary support from a Canada Research Chair (950-229395) and BCCHRI, and F.C.L. by salary support from the BCCHRI, Diabetes Canada, and the MSFHR (BIOM 5238). The funders had no role in study design, data collection and analysis, decision to publish, or preparation of the manuscript. NIH grants to Velocigene at Regeneron Inc (U01HG004085) and the CSD Consortium (U01HG004080) funded the generation of gene-targeted ES cells for 8500 genes in the KOMP Program and archived and distributed by the KOMP Repository at UC Davis and CHORI (U42RR024244). UBC and BC Children's Hospital are situated on the traditional, ancestral, and unceded territories of the Coast Salish peoples, the Sḵwx̱wú7mesh (Squamish), səl̓ilwətaʔɬ (Tsleil-Waututh), and xʷməθkʷəy̓əm (Musqueam) Nations.

Author contributions

Conceptualization, F.C.L. and S.T.; Methodology, D.S.L., F.C.L. and S.T.; Investigation, A.Z.K., B.V., S.M., R.J.S., M.D., K.Z., E.E.X., S.S., X.C., S.L.J.S., T.S., C.N., R.C., R.S., B.G.H. and F.C.L.; Writing—Original Draft, A.Z.K.; Writing—Review & Editing, F.C.L. and S.T.; Funding Acquisition, F.C.L. and S.T.; Resources, B.G.H.; Supervision, F.C.L. and S.T.

Competing interests

The authors declare no competing interests.

Additional information

Supplementary information The online version contains supplementary material available at https://doi.org/10.1038/s41467-024-52801-9.

Correspondence and requests for materials should be addressed to Stefan Taubert or Francis C. Lynn.

Peer review information *Nature Communications* thanks the anonymous reviewer(s) for their contribution to the peer review of this work. A peer review file is available.